

Designing nickelate superconductors with d^8 configuration exploiting mixed-anion strategy

Naoya Kitamine,¹ Masayuki Ochi,¹ and Kazuhiko Kuroki¹

¹*Department of Physics, Osaka University, 1-1 Machikaneyama-cho, Toyonaka, Osaka, 560-0043, Japan*
(Dated: December 2, 2020)

Inspired by a recently proposed superconducting mechanism for a new cuprate superconductor $\text{Ba}_2\text{CuO}_{3+\delta}$, we theoretically design an unconventional nickelate superconductor with a d^8 electron configuration. Our strategy is to enlarge the on-site energy difference between $3d_{x^2-y^2}$ and other $3d$ orbitals by adopting halogens or hydrogen as out-of-plane anions, so that the $3d$ bands other than $d_{x^2-y^2}$ lie just below the Fermi level for the d^8 configuration, acting as incipient bands that enhance superconductivity. We also discuss a possible relevance of the present proposal to the recently discovered superconductor $(\text{Nd,Sr})\text{NiO}_2$.

The two families of high- T_c superconductors, cuprates¹ and iron-based², are often contrasted as single-orbital vs. multi-orbital systems. Namely, in the cuprates, only the $d_{x^2-y^2}$ orbital plays the main role while in the iron-based superconductors, d_{xy} , d_{xz} , and d_{yz} orbitals largely contribute to the electronic structure around the Fermi level (E_F). Recently, however, there has occurred a possible paradigm shift to this picture, owing to some new experimental findings. One such experiment is the discovery of high- T_c superconductivity in $\text{Ba}_2\text{CuO}_{3+\delta}$, where the apical oxygen height is so low that the energy levels of $d_{x^2-y^2}$ and $d_{3z^2-r^2}$ can be reversed compared to conventional cuprates. Another example is a highly overdoped CuO_2 monolayer grown on $\text{Bi}_2\text{Sr}_2\text{CaCu}_2\text{O}_{8+\delta}$ ⁴, where E_F is significantly lowered so that it reaches the $d_{3z^2-r^2}$ band⁵.

For $\text{Ba}_2\text{CuO}_{3+\delta}$, various theoretical studies have been performed^{6–12}, many of which treat multi-orbital models. In Ref.¹², two of the present authors have introduced a two-orbital model consisting of Wannier orbitals with $d_{x^2-y^2}$ and $d_{3z^2-r^2}$ symmetries, where s -wave superconductivity with a reversed gap sign between the two bands ($s\pm$ -wave pairing) is found to be strongly enhanced near half filling when the energy level offset ΔE between $d_{3z^2-r^2}$ and $d_{x^2-y^2}$ orbitals is enlarged so that the bottom of the $d_{3z^2-r^2}$ band is positioned just above E_F . The strong enhancement of superconductivity was explained by transforming the two-orbital model to the bilayer Hubbard model, where the two orbitals of the former model correspond to the bonding and antibonding orbitals of the latter, and hence the orbital level off-

set ΔE in the former transforms to $2t_\perp$ in the latter, with t_\perp being the vertical hopping between the layers in the bilayer model, as schematically depicted in Fig.1. A more detailed explanation of this transformation is given in the supplemental material¹³. The bilayer Hubbard model has been intensively studied in the past^{15–31}, and $s\pm$ -wave superconductivity is found to be strongly enhanced near half filling when t_\perp is several times larger than the in-plane hopping and E_F lies in the vicinity of one of the bands^{15,20,25–30}. Nowadays, a band sitting just below (or above) E_F is often referred to as an incipient band, and has attracted interest in the study of iron-based superconductors^{32–39}, bilayer and ladder-type lattices^{28–31,40–44}, and flat-band superconductivity^{45–48}. The two-orbital to bilayer transformation is mathematically exact when there is no hybridization between the two orbitals and also $U = U' = J = J'$ is satisfied, where U , U' , J , and J' are the intraorbital repulsion, interorbital repulsion, Hund's coupling, and the pair hopping interaction, respectively^{12,49}. In reality, $U > U' > J, J'$ and the interorbital hybridization is present, but the analogy between the two models turns out to be approximately valid even in the realistic situation¹².

Actually, a situation where E_F lies close to the $d_{3z^2-r^2}$ band edge is realized in a cuprate $(\text{La,Sr})_2\text{CuO}_4$. One of the present authors and his colleagues have pointed out that the presence of the $d_{3z^2-r^2}$ band around E_F is the origin of the *suppression* of T_c of the d -wave superconductivity in this material^{50–53} due to the orbital component mixture around the antinodal regime. The difference between $(\text{La,Sr})_2\text{CuO}_4$ and $\text{Ba}_2\text{CuO}_{3+\delta}$ in Ref.¹² is that in the former, the e_g bands are close to 3/4 filling on average (nearly two electrons in $d_{3z^2-r^2}$ and one electron in $d_{x^2-y^2}$), while the latter is closer to half filling.

The above consideration brings us to an idea of realizing incipient-band-enhanced superconductivity in *nickelates*, where the e_g bands become half filled on average for the natural Ni^{2+} valence, namely, the d^8 electron configuration. Actually, if all the bands other than $d_{x^2-y^2}$ sink below E_F for the d^8 configuration, a pair of $d_{x^2-y^2}$ and any other d orbital is half filled (two electrons per two orbital on average), so if a small amount of electrons is doped into such systems, we may expect

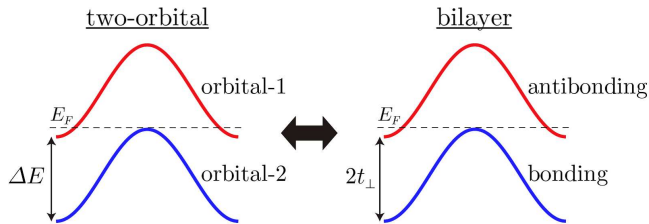


FIG. 1: A schematic image of the equivalence between the two-orbital model and the bilayer model.

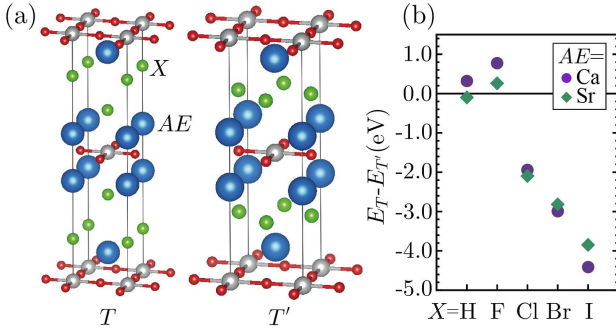


FIG. 2: (a) T and T' crystal structures. (b) The total energy difference per formula unit between T and T' structures for various choices of elements.

enhanced $s\pm$ -wave superconductivity. To enlarge the energy level offset between $d_{x^2-y^2}$ and $d_{3z^2-r^2}$ orbitals, we adopt a mixed-anion strategy⁵⁴, namely, we chose halogens or hydrogens instead of oxygens as out-of-plane anions (which corresponds to enhancing t_\perp in the bilayer system), for which we end up with the composition of $AE_2\text{NiO}_2X_2$ ($AE=\text{Ca, Sr}$, $X=\text{H, F, Cl, Br, I}$)⁵⁵.

We note that similar materials have been proposed in Ref.⁵⁶ in the context of a recently discovered superconductor $(\text{Nd, Sr})\text{NiO}_2$ ⁵⁷, but there, the aim was to construct ideal single-band systems with a d^9 electron configuration, where bands other than Ni $d_{x^2-y^2}$ do not intersect E_F for the mother compound. In fact, here we later conversely discuss a possible relevance of the present d^8 proposal to the superconductivity of $(\text{Nd, Sr})\text{NiO}_2$.

We consider $T(\text{K}_2\text{NiO}_4)$ and T' (Fig.2) structures as candidates for possible crystal structures⁵⁸. We also take La_2NiO_4 (T structure) as a reference with a d^8 configuration. We perform a structural optimization adopting the PBE-GGA exchange-correlation functional⁵⁹ and the projector augmented-wave method⁶⁰. We use the Vienna ab initio Simulation Package (VASP)⁶¹⁻⁶⁴. A $12 \times 12 \times 12$ k mesh and a plane-wave cutoff energy of 550 eV were used. After the structural optimization, we perform a first-principles band-structure calculation using the WIEN2k code⁶⁵. We adopt RKmax=7 (6 for oxy-hydrides), and take $12 \times 12 \times 12$ k mesh in the self-consistent-field calculations. From the calculated band structures, we extract the Wannier functions^{66,67} of five Ni $3d$ orbitals using the Wien2Wannier⁶⁸ and Wannier90⁶⁹ codes. Throughout the study, the spin-orbit coupling is neglected.

In Fig.2(b), we plot the total energy difference between the two structures for all choices of AE and X elements. It is found that for $X=\text{Cl, Br}$ and I , the T structure has lower energy ($E_T - E_{T'} < 0$), while the difference between the two is small for $X=\text{H, F}$. In fact, the phonon calculation of $\text{Ba}_{0.5}\text{La}_{0.5}\text{NiO}_2\text{F}_2$ in Ref.⁵⁶ shows the appearance of imaginary modes for the T structure, but not for T' , which suggests stability of the latter. The optimized lattice constants presented in the supplemental material exhibit a trend where the in-plane lattice con-

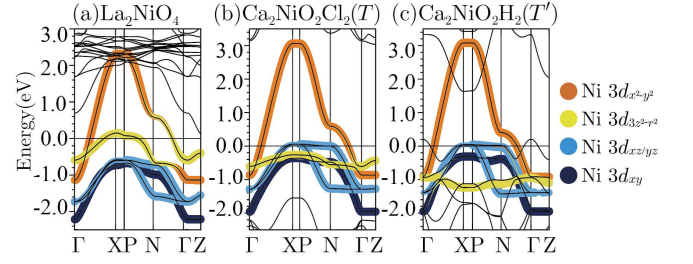


FIG. 3: The band structures of (a) La_2NiO_4 , (b) $\text{Ca}_2\text{NiO}_2\text{Cl}_2$ (T), and (c) $\text{Ca}_2\text{NiO}_2\text{H}_2$ (T'). The band dispersion of the five orbital model is superposed to the first principles bands.

stant a becomes larger as the ion radius of element X or AE is increased¹³.

The first-principles band structures obtained for the optimized lattice structures of La_2NiO_4 (T), $\text{Ca}_2\text{NiO}_2\text{Cl}_2$ (T), and $\text{Ca}_2\text{NiO}_2\text{H}_2$ (T') are shown in Fig.3. The energy dispersion of the five-orbital model is superposed to the first-principles bands for each material. The band structures of materials with other elements are presented in the supplemental material¹³. It can be noticed that in the mixed-anion materials, the $d_{3z^2-r^2}$ band totally sinks below E_F despite the d^8 electron configuration with the $d_{x^2-y^2}$ band partially filled, in sharp contrast to the case of La_2NiO_4 . The entire d_{xy} band also lies below E_F , while the top of the $d_{xz/yz}$ bands intersects E_F .

In Fig.4, we plot the on-site energy (ΔE) of the d orbitals with respect to that of $d_{x^2-y^2}$ in the five-orbital model. Let us focus on the crystal structure having the lower total energy (denoted by the solid symbols). $|\Delta E|$ tends to be larger (i.e., the energy level is lowered since $\Delta E < 0$) as the ion radius of X is reduced within $X=\text{Cl, Br}$ and I . This is due to the smaller in-plane lattice constant (shorter Ni-O distance), which pushes up the $d_{x^2-y^2}$ energy level. For the T' structure, the on-site energy of the $d_{3z^2-r^2}$ orbital is strongly reduced due to the absence of the apical anions, but the t_{2g} orbitals are pushed up compared to those in the T structure. If we compare $AE=\text{Sr}$ and Ca , $|\Delta E|$ of the t_{2g} orbitals are reduced in the former compared to the latter, while that of $d_{3z^2-r^2}$ is less affected. This is because the lattice constants a and c are shorter for $AE=\text{Ca}$ than for Sr .

We now analyze superconductivity based on the obtained five-orbital models. We assume on-site intra- and interorbital interactions, U , U' , J and J' , and the many-body study of this model is performed within the fluctuation exchange approximation (FLEX)⁷⁰. We mainly adopt $U = 4\text{eV}$, $J = J' = U/8$, $U' = U - 2J$, but also discuss the interaction dependence in the supplemental material¹³. A relatively large U is taken in accord with a study for LaNiO_2 ⁷³. We obtain the renormalized Green's function by solving the Dyson's equation in a self-consistent calculation. The obtained Green's function and the pairing interaction mediated mainly by spin fluctuations are plugged into the linearized Eliashberg equation. Since the eigenvalue λ of the equation reaches

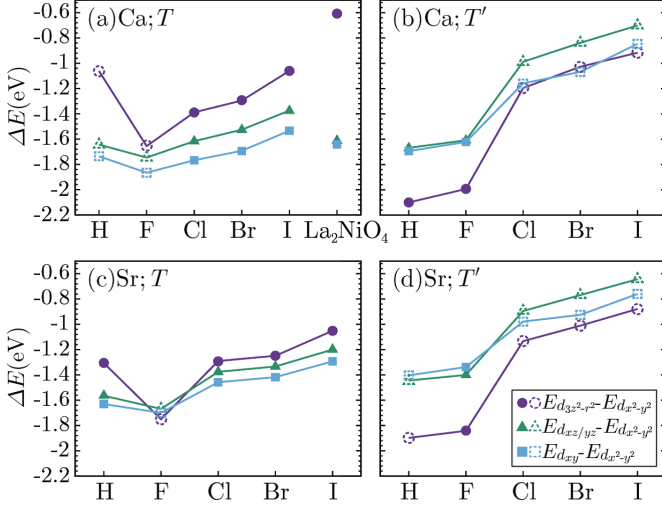


FIG. 4: The on-site energy of the d orbitals other than the $d_{x^2-y^2}$ orbital, measured from that of $d_{x^2-y^2}$. (a) $AE=Ca; T$, (b) $Ca; T'$, (c) $Sr; T$, and (d) $Sr; T'$. Here, the solid (dashed) symbols denote the lattice structure with lower (higher) total energy. As a reference, the values of ΔE for La_2NiO_4 are plotted in (a).

unity at $T = T_c$, here we adopt λ , obtained at a fixed temperature of $T = 0.01\text{eV}$, to measure how close the system is to superconductivity. The eigenfunction of the Eliashberg equation will be called the gap function. In the FLEX calculation, a $16 \times 16 \times 4$ (k_x, k_y, k_z) mesh and 2048 Matsubara frequencies were taken.

In Figs.5(a) and 5(b), we plot the eigenvalue of the Eliashberg equation against the band filling, varied assuming a rigid band, for various materials with the crystal structure (T or T') having a lower total energy. In all mixed-anion compounds, λ is peaked at around $n = 4.1$ to 4.2 , which corresponds to 10 to 20% electron doping starting from the stoichiometric band filling of $n = 4$. The compounds having the largest maximum λ are $Ca_2NiO_2Cl_2$ and $Ca_2NiO_2H_2$. These maximum values of λ are much larger compared to that of La_2NiO_4 ⁷⁵, and they are in fact even larger than that of $HgBa_2CuO_4$, a $T_c = 100\text{K}$ superconductor, obtained in the same manner⁷³. It is also worth mentioning that the Stoner factor for magnetic ordering remains far from unity for the situation when λ of superconductivity is optimized, which is typical for the incipient-band-enhanced superconductivity (see supplemental material¹³).

The gap function presented in Fig.5(c) for the case of $Ca_2NiO_2Cl_2$ with $n = 4.125$ shows that the four bands other than $d_{x^2-y^2}$ have the same sign of the gap, opposite to that of the $d_{x^2-y^2}$ band (see the supplemental material for the contour plot of the gap¹³). In this sense, this is $s\pm$ -wave pairing with the four bands other than $d_{x^2-y^2}$ being incipient, namely, located below E_F , with the $d_{xz/yz}$ band top being the closest to E_F . In order to see the role played by each orbital in more detail, we extract one, three, or four orbitals from the five-orbital

model, and apply FLEX to those models to obtain λ in a similar manner, as depicted in Fig.5(d). The comparison among the models is made at the same electron doping rates, since the Fermi surfaces are the same among the multi-orbital models that contain the $d_{xz/yz}$ orbitals. The $d_{x^2-y^2}$ Fermi surfaces of the multi-orbital models are also (nearly) the same as that of the single-band model in the relevant band-filling regime, as explained in more detail in the supplemental material¹³.

From Fig.5(d), it can be seen that λ in the $d_{x^2-y^2} + d_{xz/yz}$ model is strongly enhanced compared to the single-orbital model consisting only of $d_{x^2-y^2}$, indicating the important role played by the incipient $d_{xz/yz}$ bands. Adding d_{xy} to the $d_{x^2-y^2} + d_{xz/yz}$ model somewhat enhances λ , but not drastically. Our interpretation for this is that the interaction between d_{xy} and $d_{x^2-y^2}$ orbitals enhances superconductivity because the signs of the gap are opposite, but the interaction between d_{xy} and $d_{xz/yz}$ gives a negative contribution to superconductivity because of the same sign of the gap. On the other hand, adding the $d_{3z^2-r^2}$ orbital to the $d_{x^2-y^2} + d_{xz/yz}$ model even slightly suppresses λ . An argument similar to d_{xy} should apply also to $d_{3z^2-r^2}$, but, in addition, we find that the hybridization between $d_{3z^2-r^2}$ and $d_{x^2-y^2}$ (note that the $d_{x^2-y^2}$ orbital is hybridized only with $d_{3z^2-r^2}$) gives a negative contribution to superconductivity, similarly to what has already been known for the cuprates⁵⁰⁻⁵³. It is also interesting to note that the $d_{3z^2-r^2}$ gap function has the largest value among

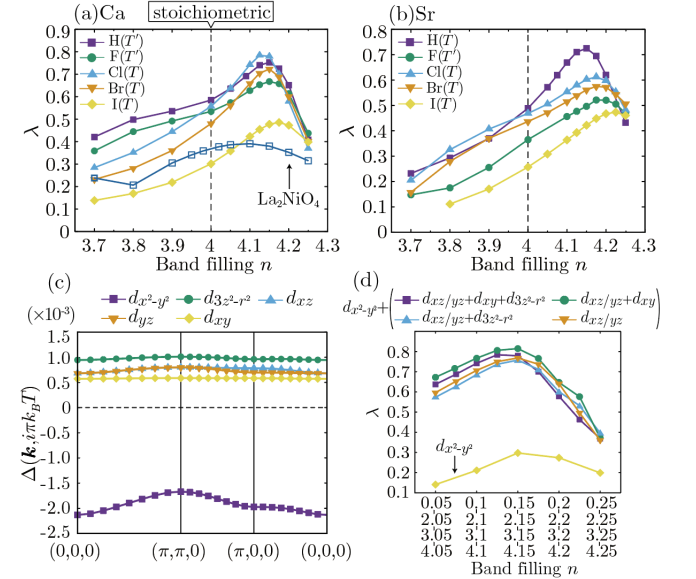


FIG. 5: Eigenvalue of the Eliashberg equation λ at $T = 0.01\text{eV}$ against the band filling for (a) $AE=Ca$ and (b) Sr . In (a), also the results for La_2NiO_4 are plotted as a reference. (c) Gap function of $Ca_2NiO_2Cl_2$ for $n = 4.125$ in the orbital representation. (d) Similar plot of λ obtained for various one-, three-, and four-orbital models (see text) of $Ca_2NiO_2Cl_2$. The horizontal axis is the band filling (for the single-orbital to the five-orbital model from top to bottom).

the incipient bands, despite the negative contribution of $d_{3z^2-r^2}$ to λ , and also despite the $d_{3z^2-r^2}$ band lying somewhat away from E_F compared to the top of the $d_{xz/yz}$ bands. We believe that this is a consequence of small $|\Delta E|$ for $d_{3z^2-r^2}$ orbital in $\text{Ca}_2\text{NiO}_2\text{Cl}_2$, which implies that this band lies closest to E_F among the incipient bands as far as the center of gravity of the band is concerned. More detailed analyses on these issues are given in the supplemental material¹³.

Since λ is dominated by the position of the $d_{xz/yz}$ bands, the materials having a larger energy difference between the $d_{x^2-y^2}$ and $d_{xz/yz}$ orbitals, corresponding to larger t_\perp in the bilayer Hubbard model¹², tend to exhibit larger λ . On the other hand, it should be stressed that the strong reduction of λ for La_2NiO_4 compared to mixed-anion materials mainly comes from the small $|\Delta E|$ for the $d_{3z^2-r^2}$ orbital; the $d_{3z^2-r^2}$ band intersecting E_F gives rise to the strong development of low-energy spin fluctuations, which works destructively against superconductivity, as in the case of the bilayer Hubbard model with small t_\perp ^{26,27,29,30}. A further analysis on the role played by each orbital is given in the supplemental material¹³.

We note that all of our calculations assume a low-spin state, while nickelates with a d^8 configuration can take high-spin states when the d -level splittings are small. In fact, the reference system in our study La_2NiO_4 is actually well known to be in the high-spin state, and also $\text{Sr}_2\text{NiO}_2\text{Cl}_2$, synthesized in Ref.⁷¹, was found to be in a high-spin state. On the other hand, a hypothetical infinite layer nickelate SrNiO_2 , without apical anions, was theoretically shown to have a low-spin ground state⁷². Hence, large $|\Delta E|$ is not only preferable for enhancing T_c , but it is also favorable from the viewpoint of realizing a low-spin ground state. In this sense, $\text{AE}=\text{Ca}$ rather than Sr and also $\text{X}=\text{Cl}$ rather than Br or I (T structure) is likely to be the best choice from the viewpoint of both realizing a low-spin state and enhancing T_c because of the smaller in-plane lattice constant and hence larger $|\Delta E|$. Our result indicates that superconductivity in $\text{AE}_2\text{NiO}_2\text{X}_2$ is optimized by electron doping, which may be realized in actual materials by, e.g., partially substituting Ca^{2+} (or Sr^{2+}) with La^{3+} . In fact, a pure d^8 configuration (band filling of $n = 4$) may result in an insulating state not predicted within the present calculation. Electron doping should prevent the material from being an insulator, and hence may also stabilize the preferred low-spin state in actual materials. In total, the materials we propose here as candidates for new unconventional superconductors have the composition forms $\text{Ca}_{2-x}\text{La}_x\text{NiO}_2\text{Cl}_2$ and $\text{Ca}_{2-x}\text{La}_x\text{NiO}_2\text{H}_2$.

Now, if we increase the amount of electron doping in the present materials, they approach the materials with a d^9 electron configuration studied in Refs.^{56,74} in the context of a recently discovered superconductor $(\text{Nd,Sr})\text{NiO}_2$ ⁵⁷. Then, conversely, it is interesting to see how the d^9 and d^8 states are connected in $(\text{Nd,Sr})\text{NiO}_2$ by hypothetically removing the electrons. Here, we consider

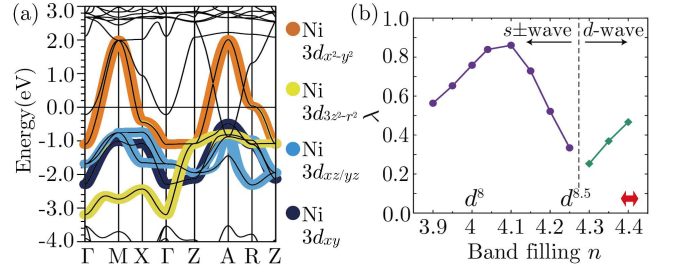


FIG. 6: (a) The first principles band structure of LaNiO_2 with the five-orbital model superposed. (b) λ against the band filling for the model of LaNiO_2 . \leftrightarrow shows the band filling-regime corresponding to the Sr content where superconductivity is observed in Refs.^{82,83} assuming no residual hydrogens are present.

LaNiO_2 adopting the experimentally determined lattice parameters of NdNiO_2 to avoid the ambiguity regarding the treatment of the f electrons in Nd ⁷³. Since a previous study has shown that the La 5d orbitals have a small effect on spin-fluctuation-mediated superconductivity⁷³, we construct a five Ni-3d-orbital model similar to those for $\text{AE}_2\text{NiO}_2\text{X}_2$, as shown in Fig.6(a). The band structure somewhat resembles that of $\text{AE}_2\text{NiO}_2\text{Cl}_2$ in that the position of the $d_{3z^2-r^2}$ band is lowered, which is because the apical anions are absent in this infinite layer material, but the difference lies in that the $d_{3z^2-r^2}$ band exhibits strong three dimensionality. We perform a similar FLEX analysis of superconductivity for this model by hypothetically varying the band filling assuming a rigid band. As expected from our results on $\text{AE}_2\text{NiO}_2\text{X}_2$, there appears a peak in λ close to $n = 4$, i.e., the d^8 configuration, in addition to the already known d -wave superconductivity around $n = 4.5$, the d^9 configuration.

Although we believe that the mechanism similar to the cuprates, where only the $d_{x^2-y^2}$ band plays an important role, is a strong candidate for the superconducting mechanism of $(\text{Nd,Sr})\text{NiO}_2$ ^{73,76-78}, the present analysis suggests that their might be an alternative scenario where Ni 3d orbitals other than $d_{x^2-y^2}$ play the role of incipient bands. In fact, as studied in Ref.⁷⁹, $(\text{Nd,Sr})\text{NiO}_2\text{H}$ may form during the reduction process by CaH_2 , which would reduce the number of d electrons⁸⁰. Another theoretical study shows that a similar situation can occur also at the SrTiO_3 substrate interface⁸¹. In Fig.6(b), we indicate the band-filling regime corresponding to the Sr content where superconductivity is observed in Refs.^{82,83} assuming no residual hydrogens are present. This region will be shifted by $p/2$ toward the smaller band-filling regime if residual hydrogens are present in the form $(\text{Nd,Sr})\text{NiO}_2\text{H}_p$. It will then be an interesting future problem to carefully examine the Ni valence in $(\text{Nd,Sr})\text{NiO}_2$. Also, the gap function would be of interest since the d wave should be realized for the d^9 pairing mechanism, whereas the s wave is expected for the d^8 scenario. In fact, while finalizing the present paper, a tunneling spectroscopy experiment has been reported⁸⁴,

where s -wave and d -wave-like gaps have been observed, depending on the position on the sample. The experiment has been interpreted in terms of the gap with a different symmetry opening on different Fermi surfaces, which was suggested theoretically⁸⁵. From our viewpoint, the position dependence of the pairing symmetry might originate from the inhomogeneity of the residual hydrogen remained during the reduction process⁸⁶.

To conclude, we have designed unconventional nickelate superconductors with a nearly d^8 electron configuration, where superconductivity is enhanced by the bands other than $d_{x^2-y^2}$ playing a role of the incipient bands. The key idea is to exploit the mixed-anion strategy to enlarge the on-site energy difference between $d_{x^2-y^2}$ and other d orbitals. This corresponds to increasing the interlayer hopping t_{\perp} of the bilayer Hubbard model, which is known to exhibit $s\pm$ -wave superconductivity strongly enhanced by the incipient-band effect for large t_{\perp} . The

possible relevance of the present proposal to the observation of superconductivity in (Nd,Sr)NiO₂ is an interesting future problem, where a non-rigid-band variation of the incipient-band dispersion due to residual hydrogens⁷⁹ should be taken into account.

Acknowledgments

We acknowledge Kimihiro Yamazaki, Hirofumi Sakakibara, and Hideo Aoki for valuable discussions. Parts of the numerical calculations were performed at the Supercomputer Center, Institute for Solid State Physics, University of Tokyo. This study has been supported by JSPS KAKENHI Grant Numbers JP18H01860, JP19H04697, and JP19H05058.

-
- ¹ For a review, see e.g. B. Keimer, S. A. Kivelson, M. R. Norman, S. Uchida, and J. Zaanen, From quantum matter to high-temperature superconductivity in copper oxides, *Nature* **518**, 179 (2015).
 - ² For a review, see e.g., H. Hosono and K. Kuroki, Iron-based superconductors: Current status of materials and pairing mechanism, *Physica C* **514**, 399 (2015).
 - ³ W. M. Li, J. F. Zhao, L. P. Cao, Z. Hu, Q. Z. Huang, X. C. Wang, Y. Liu, G. Q. Zhao, J. Zhang, Q. Q. Liu, R. Z. Yu, Y. W. Long, H. Wu, H. J. Lin, C. T. Chen, Z. Li, Z. Z. Gong, Z. Guguchia, J. S. Kim, G. R. Stewart, Y. J. Uemura, S. Uchida, and C. Q. Jin, Superconductivity in a unique type of copper oxide, *Proc. Natl. Acad. Sci. U.S.A.* **116**, 12156 (2019).
 - ⁴ Y. Zhong, Y. Wang, S. Han, Y. Lv, W. Wang, D. Zhang, H. Ding, Y. Zhang, L. Wang, K. He, R. Zhong, J. A. Schneeloch, G. Gu, C. Song, X. Ma, and Q. K. Xue, Nodeless pairing in superconducting copper-oxide monolayer films on Bi₂Sr₂CaCu₂O_{8+ δ} , *Sci. Bull.* **61**, 1239 (2016).
 - ⁵ K. Jiang, X. Wu, J. Hu, and Z. Wang, Nodeless high- T_c superconductivity in the highly overdoped CuO₂ monolayer, *Phys. Rev. Lett.* **121**, 227002 (2018).
 - ⁶ T. Maier, T. Berlijn, and D. J. Scalapino, Two pairing domes as Cu²⁺ varies to Cu³⁺, *Phys. Rev. B* **99**, 224515 (2019).
 - ⁷ K. Liu, Z. Y. Lu, and T. Xiang, Electronic structures of quasi-one-dimensional cuprate superconductors Ba₂CuO_{3+ δ} , *Phys. Rev. Materials* **3**, 044802 (2019).
 - ⁸ C. Le, K. Jiang, Y. Li, S. Qin, Z. Wang, F. Zhang, and J. Hu, Electronic structure and superconductivity in unconventional cuprates Ba₂CuO_{3+ δ} , arXiv:1909.12620.
 - ⁹ Y. Li, S. Du, Z.-Y. Weng, and Z. Liu, In-plane ordering of oxygen vacancies in a high- T_c cuprate superconductor with compressed Cu-O octahedrons: An automated cluster expansion study, *Phys. Rev. Materials* **4**, 044801 (2020).
 - ¹⁰ Y. Ni, Y.-M. Quan, J. Liu, Y. Song, and L.-J. Zou, Electronic correlation driven orbital polarization transitions in the orbital-selective Mott compound Ba₂CuO_{4- δ} , arXiv:1912.10580 (2019).
 - ¹¹ Z. Wang, S. Zhou, W. Chen, and F.-C. Zhang, $t - J$ model on the effective brick-wall lattice for the recently discovered high-temperature superconductor Ba₂CuO_{3+ δ} , *Phys. Rev. B* **101**, 180509(R) (2020).
 - ¹² K. Yamazaki, M. Ochi, D. Ogura, K. Kuroki, H. Eisaki, S. Uchida, and H. Aoki, Superconducting mechanism for the cuprate Ba₂CuO_{3+ δ} based on a multiorbital Lieb lattice model, *Phys. Rev. Research* **2**, 033356 (2020).
 - ¹³ See Supplemental Material for details, which includes Ref.¹⁴ not cited in the main text.
 - ¹⁴ R. Arita, K. Kuroki, and H. Aoki, d - and p -wave superconductivity mediated by spin fluctuations in two- and three-dimensional single-band repulsive Hubbard model, *J. Phys. Soc. Jpn.* **69**, 1181 (2000).
 - ¹⁵ N. Bulut, D. J. Scalapino, and R. T. Scalettar, Nodeless d -wave pairing in a two-layer Hubbard model, *Phys. Rev. B* **45**, 5577 (1992).
 - ¹⁶ R. T. Scalettar, J. W. Cannon, D. J. Scalapino, and R. L. Sugar, Magnetic and pairing correlations in coupled Hubbard planes, *Phys. Rev. B* **50**, 13419 (1994).
 - ¹⁷ R. E. Hetzel, W. von der Linden, and W. Hanke, Pairing correlations in a two-layer Hubbard model, *Phys. Rev. B* **50**, 4159 (1994).
 - ¹⁸ R. R. dos Santos, Magnetism and pairing in Hubbard bilayers, *Phys. Rev. B* **51**, 15540 (1995).
 - ¹⁹ A. I. Liechtenstein, I. I. Mazin, and O. K. Andersen, s -wave superconductivity from an antiferromagnetic spin-fluctuation model for bilayer materials, *Phys. Rev. Lett.* **74**, 2303 (1995).
 - ²⁰ K. Kuroki, T. Kimura, and R. Arita, High-temperature superconductivity in dimer array systems, *Phys. Rev. B* **66**, 184508 (2002).
 - ²¹ S. S. Kancharla and S. Okamoto, Band insulator to Mott insulator transition in a bilayer Hubbard model, *Phys. Rev. B* **75**, 193103 (2007).
 - ²² K. Bouadim, G. G. Batrouni, F. Hebert, and R. T. Scalettar, Magnetic and transport properties of a coupled Hubbard bilayer with electron and hole doping, *Phys. Rev. B* **77**, 144527 (2008).
 - ²³ N. Lanata, P. Barone, and M. Fabrizio, Superconductivity in the doped bilayer Hubbard model, *Phys. Rev. B* **80**,

- 224524 (2009).
- ²⁴ H. Zhai, F. Wang, and D.-H. Lee, Antiferromagnetically driven electronic correlations in iron pnictides and cuprates, *Phys. Rev. B* **80**, 064517 (2009).
 - ²⁵ T. A. Maier and D. J. Scalapino, Pair structure and the pairing interaction in a bilayer Hubbard model for unconventional superconductivity, *Phys. Rev. B* **84**, 180513(R) (2011).
 - ²⁶ V. Mishra, D. J. Scalapino, and T. A. Maier, $s\pm$ pairing near a Lifshitz transition, *Sci. Rep.* **6**, 32078 (2016).
 - ²⁷ M. Nakata, D. Ogura, H. Usui, and K. Kuroki, Finite-energy spin fluctuations as a pairing glue in systems with coexisting electron and hole bands, *Phys. Rev. B* **95**, 214509 (2017).
 - ²⁸ T. A. Maier, V. Mishra, G. Balduzzi, and D. J. Scalapino, Effective pairing interaction in a system with an incipient band, *Phys. Rev. B* **99**, 140504(R) (2019).
 - ²⁹ K. Matsumoto, D. Ogura and K. Kuroki, Strongly enhanced superconductivity due to finite energy spin fluctuations induced by an incipient band: A FLEX study on the bilayer Hubbard model with vertical and diagonal interlayer hoppings, *J. Phys. Soc. Jpn.* **89**, 044709 (2020).
 - ³⁰ D. Kato and K. Kuroki, Many-variable variational Monte Carlo study of superconductivity in two-band Hubbard models with an incipient band, *Phys. Rev. Research* **2**, 023156 (2020).
 - ³¹ M. Kainth and M. W. Long, A rigorous demonstration of superconductivity in a repulsive Hubbard model, arXiv:1904.07138.
 - ³² A. Charnukha, D. V. Evtushinsky, C. E. Matt, N. Xu, M. Shi, B. Büchner, N. D. Zhigadlo, B. Batlogg, and V. Borisenko, High-temperature superconductivity from fine-tuning of Fermi-surface singularities in iron oxypnictides, *Sci. Rep.* **5**, 18273 (2015).
 - ³³ H. Miao, T. Qian, X. Shi, P. Richard, T. K. Kim, M. Hoesch, L. Y. Xing, X.-C. Wang, C.-Q. Jin, J.-P. Hu, and H. Ding, Observation of strong electron pairing on bands without Fermi surfaces in $\text{LiFe}_{1-x}\text{Co}_x\text{As}$, *Nat. Commun.* **6**, 6056 (2015).
 - ³⁴ F. Wang, F. Yang, M. Gao, Z.-Y. Lu, T. Xiang, and D.-H. Lee, The electron pairing of $\text{K}_x\text{Fe}_{2-y}\text{Se}_2$, *Europhys. Lett.* **93**, 57003 (2011).
 - ³⁵ Y. Bang, A shadow gap in the over-doped $(\text{Ba}_{1-x}\text{K}_x)\text{Fe}_2\text{As}_2$ compound, *New J. Phys.* **16**, 023029 (2014).
 - ³⁶ X. Chen, S. Maiti, A. Linscheid, and P. J. Hirschfeld, Electron pairing in the presence of incipient bands in iron-based superconductors, *Phys. Rev. B* **92**, 224514 (2015).
 - ³⁷ P. J. Hirschfeld, M. M. Korshunov and I. I. Mazin, Gap symmetry and structure of Fe-based superconductors, *Rep. Prog. Phys.* **74**, 124508 (2011).
 - ³⁸ Y. Bang, Pairing mechanism of heavily electron doped FeSe systems: dynamical tuning of the pairing cutoff energy, *New J. Phys.* **18**, 113054 (2016).
 - ³⁹ Y. Bang, Phonon boost effect on the $s\pm$ -wave superconductor with incipient band, *Sci. Reports* **9**, 3907 (2019).
 - ⁴⁰ K. Kuroki, T. Higashida, and R. Arita, High- T_c superconductivity due to coexisting wide and narrow bands: A fluctuation exchange study of the Hubbard ladder as a test case, *Phys. Rev. B* **72**, 212509 (2005).
 - ⁴¹ K. Matsumoto, D. Ogura, and K. Kuroki, Wide applicability of high- T_c pairing originating from coexisting wide and incipient narrow bands in quasi-one-dimensional systems, *Phys. Rev. B* **97**, 014516(2018).
 - ⁴² D. Ogura, H. Aoki, K. Kuroki, Possible high- T_c superconductivity due to incipient narrow bands originating from hidden ladders in Ruddlesden-Popper compounds, *Phys. Rev. B* **96**, 184513 (2017).
 - ⁴³ D. Ogura, Springer Theses, "Theoretical study of electron correlation driven superconductivity in systems with coexisting wide and narrow bands", Springer (2019).
 - ⁴⁴ H. Sakamoto and K. Kuroki, Possible enhancement of superconductivity in ladder-type cuprates by longitudinal compression, *Phys. Rev. Research* **2**, 022055(R) (2020).
 - ⁴⁵ K. Kobayashi, M. Okumura, S. Yamada, M. Machida, and H. Aoki, Superconductivity in repulsively interacting fermions on a diamond chain: Flat-band-induced pairing, *Phys. Rev. B* **94**, 214501 (2016).
 - ⁴⁶ T. Misumi and H. Aoki, New class of flat-band models on tetragonal and hexagonal lattices: Gapped versus crossing flat bands, *Phys. Rev. B* **96**, 155137 (2017).
 - ⁴⁷ S. Sayyad, E. W. Huang, M. Kitatani, M.-S. Vaezi, Z. Nussinov, A. Vaezi, and H. Aoki, Pairing and non-Fermi liquid behavior in partially flat-band systems: Beyond nesting physics, *Phys. Rev. B* **101**, 014501 (2020).
 - ⁴⁸ H. Aoki, Theoretical possibilities for flat band superconductivity, *J. Supercond. Novel Magn.* **33**, 2341 (2020).
 - ⁴⁹ H. Shinaoka, Y. Nomura, S. Biermann, M. Troyer, and P. Werner, Negative sign problem in continuous-time quantum Monte Carlo: Optimal choice of single-particle basis for impurity problems, *Phys. Rev. B* **92**, 195126 (2015).
 - ⁵⁰ H. Sakakibara, H. Usui, K. Kuroki, R. Arita, and H. Aoki, Two-orbital model explains the higher transition temperature of the single-layer Hg-cuprate superconductor compared to that of the La-cuprate superconductor, *Phys. Rev. Lett.* **105**, 057003 (2010).
 - ⁵¹ H. Sakakibara, H. Usui, K. Kuroki, R. Arita, and H. Aoki, Origin of the material dependence of T_c in the single-layered cuprates, *Phys. Rev. B* **85**, 064501 (2012).
 - ⁵² H. Sakakibara, K. Suzuki, H. Usui, K. Kuroki, R. Arita, D. J. Scalapino, and H. Aoki, Multiorbital analysis of the effects of uniaxial and hydrostatic pressure on T_c in the single-layered cuprate superconductors, *Phys. Rev. B* **86**, 134520 (2012).
 - ⁵³ H. Sakakibara, K. Suzuki, H. Usui, S. Miyao, I. Maruyama, K. Kusakabe, R. Arita, H. Aoki, and K. Kuroki, Orbital mixture effect on the Fermi-surface- T_c correlation in the cuprate superconductors: Bilayer vs. single layer, *Phys. Rev. B* **89**, 224505 (2014).
 - ⁵⁴ For a review on mixed-anion compounds, see, H. Kageyama, K. Hayashi, K. Maeda, J. P. Attfield, Z. Hiroi, J. M. Rondinelli, and K. R. Poeppelmeier, Expanding frontiers in materials chemistry and physics with multiple anions, *Nat. Comm.* **9**, 772 (2018).
 - ⁵⁵ As nickelates with anions other than oxygen, F. Bernardini, V. Olevano, X. Blase, and A. Cano, Infinite-layer fluoro-nickelates as d^9 model materials, *J. Phys. Mater.* **3**, 035003 (2020) theoretically studies an infinite-layer fluoro-nickelates.
 - ⁵⁶ M. Hirayama, T. Tadano, Y. Nomura, and R. Arita, Materials design of dynamically stable d^9 layered nickelates, *Phys. Rev. B* **101**, 075107 (2020).
 - ⁵⁷ D. Li, K. Lee, B. Y. Wang, M. Osada, S. Crossley, H. R. Lee, Y. Cui, Y. Hikita, and H. Y. Hwang, Superconductivity in an infinite-layer nickelate, *Nature* **572**, 624 (2019).
 - ⁵⁸ One of the reasons we consider these structures is because they are well known in cuprates. Further estimation of their stability as nickelates is left for future study.

- ⁵⁹ J. P. Perdew, K. Burke, and M. Ernzerhof, Generalized gradient approximation made simple, *Phys. Rev. Lett.* **77**, 3865 (1996).
- ⁶⁰ G. Kresse and D. Joubert, From ultrasoft pseudopotentials to the projector augmented-wave method, *Phys. Rev. B* **59**, 1758 (1999).
- ⁶¹ G. Kresse and J. Hafner, Ab initio molecular dynamics for liquid metals, *Phys. Rev. B* **47**, 558(R) (1993).
- ⁶² G. Kresse and J. Hafner, Ab initio molecular-dynamics simulation of the liquid-metal–amorphous-semiconductor transition in germanium, *Phys. Rev. B* **49**, 14251 (1994).
- ⁶³ G. Kresse and J. Furthmüller, Efficiency of ab-initio total energy calculations for metals and semiconductors using a plane-wave basis set, *Comput. Mater. Sci.* **6**, 15 (1996).
- ⁶⁴ G. Kresse and J. Furthmüller, Efficient iterative schemes for ab initio total-energy calculations using a plane-wave basis set, *Phys. Rev. B* **54**, 11169 (1996).
- ⁶⁵ P. Blaha, K. Schwarz, G. K. H. Madsen, D. Kvasnicka, J. Luitz, R. Laskowski, F. Tran, and L. D. Marks, WIEN2k, An Augmented Plane Wave + Local Orbitals Program for Calculating Crystal Properties (Karlheinz Schwarz, Techn. Universität Wien, Austria, 2018). ISBN 3-9501031-1-2.
- ⁶⁶ N. Marzari and D. Vanderbilt, Maximally localized generalized Wannier functions for composite energy bands, *Phys. Rev. B* **56**, 12847 (1997).
- ⁶⁷ I. Souza, N. Marzari, and D. Vanderbilt, Maximally localized Wannier functions for entangled energy bands, *Phys. Rev. B* **65**, 035109 (2001).
- ⁶⁸ J. Kunes, R. Arita, P. Wissgott, A. Toschi, H. Ikeda, and K. Held, Wien2wannier: From linearized augmented plane waves to maximally localized Wannier functions, *Comput. Phys. Commun.* **181**, 1888 (2010).
- ⁶⁹ A. A. Mostofi, J. R. Yates, Y.-S. Lee, I. Souza, D. Vanderbilt, and N. Marzari, wannier90: A tool for obtaining maximally-localised Wannier functions, *Comput. Phys. Commun.* **178**, 685 (2008).
- ⁷⁰ N. E. Bickers, D. J. Scalapino, and S. R. White, Conserving approximations for strongly correlated electron systems: Bethe-Salpeter equation and dynamics for the two-dimensional Hubbard model, *Phys. Rev. Lett.* **62**, 961(1989).
- ⁷¹ Y. Tsujimoto, C. I. Sathish, Y. Matsushita, K. Yamaura, and T. Uchikoshi, New members of layered oxychloride perovskites with square planar coordination: $\text{Sr}_2\text{MO}_2\text{Cl}_2$ ($M = \text{Mn}, \text{Ni}$) and $\text{Ba}_2\text{PdO}_2\text{Cl}_2$, *Chem. Commun.* **50** 5915 (2014).
- ⁷² V. I. Anisimov, D. Bukhalov, and T.M. Rice, Electronic structure of possible nickelate analogs to the cuprates, *Phys. Rev. B* **59**, 7901 (1999).
- ⁷³ H. Sakakibara, H. Usui, K. Suzuki, T. Kotani, H. Aoki, and K. Kuroki, Model construction and a possibility of cupratelike pairing in a new d^9 nickelate superconductor (Nd,Sr)NiO₂, *Phys. Rev. Lett.* **125**, 077003 (2020).
- ⁷⁴ Y. Nomura, T. Nomoto, M. Hirayama and R. Arita, Magnetic exchange coupling in cuprate-analog d^9 nickelates, *Phys. Rev. Research* **2**, 043144 (2020).
- ⁷⁵ The five orbital model of La_2NiO_4 exhibits interorbital pairing as in Ref.¹² of $\text{Ba}_2\text{CuO}_{3+\delta}$. See the supplemental material for details.
- ⁷⁶ Y. Nomura, M. Hirayama, T. Tadano, Y. Yoshimoto, K. Nakamura, and R. Arita, Formation of a two-dimensional single-component correlated electron system and band engineering in the nickelate superconductor NdNiO₂, *Phys. Rev. B* **100**, 205138 (2019).
- ⁷⁷ M. Kitatani, L. Si, O. Janson, R. Arita, Z. Zhong, and K. Held, Nickelate superconductors—a renaissance of the one-band Hubbard model, *npj Quantum Mater.* **5**, 59 (2020).
- ⁷⁸ X. Wu, D. DiSante, T. Schwemmer, W. Hanke, H. Y. Hwang, S. Raghu, and R. Thomale, Robust $d_{x^2-y^2}$ -wave superconductivity of infinite-layer nickelates, *Phys. Rev. B* **101**, 060504(R) (2020).
- ⁷⁹ L. Si, W. Xiao, J. Kaufmann, J. M. Tomczak, Y. Lu, Z. Zhong, and K. Held, Topotactic hydrogen in nickelate superconductors and akin infinite-layer oxides ABO_2 , *Phys. Rev. Lett.* **124**, 166402 (2020).
- ⁸⁰ It is also interesting to note that the absence of superconductivity was reported in X.-R. Zhou, Z.-X. Feng, P.-X. Qin, H. Yan, S. Hu, H.-X. Guo, X.-N. Wang, H.-J. Wu, X. Zhang, H.-Yu Chen, X.-P. Qiu, and Z.-Q. Liu, Absence of superconductivity in $\text{Nd}_{0.8}\text{Sr}_{0.2}\text{NiO}_x$ thin films without chemical reduction, *Rare Met.* **39**, 368 (2020), where CaH_2 was not used to synthesize (Nd,Sr)NiO₂.
- ⁸¹ F. Bernardini and A. Cano, Stability and electronic properties of $\text{LaNiO}_2/\text{SrTiO}_3$ heterostructures, *J. Phys. Mater.* **3**, 03LT01 (2020).
- ⁸² D. Li, B. Y. Wang, K. Lee, S. P. Harvey, M. Osada, B. H. Goodge, L. F. Kourkoutis, and H. Y. Hwang, Superconducting dome in $\text{Nd}_{1-x}\text{Sr}_x\text{NiO}_2$ infinite layer films, *Phys. Rev. Lett.* **125**, 027001 (2020).
- ⁸³ S. Zeng, C. S. Tang, X. Yin, C. Li, Z. Huang, J. Hu, W. Liu, G. J. Omar, H. Jani, Z. S. Lim, K. Han, D. Wan, P. Yang, A. T. S. Wee, and A. Ariando, Phase diagram and superconducting dome of infinite-layer $\text{Nd}_{1-x}\text{Sr}_x\text{NiO}_2$ thin films, *Phys. Rev. Lett.* **125**, 147003 (2020).
- ⁸⁴ Q. Gu, Y. Li, S. Wan, H. Li, W. Guo, H. Yang, Q. Li, X. Zhu, X. Pan, Y. Nie, and H.-H. Wen, Two superconducting components with different symmetries in $\text{Nd}_{1-x}\text{Sr}_x\text{NiO}_2$ films, arXiv:2006.13123.
- ⁸⁵ P. Adhikary, S. Bandyopadhyay, T. Das, I. Dasgupta, and T. Saha-Dasgupta, Orbital-selective superconductivity in a two-band model of infinite-layer nickelates, *Phys. Rev. B* **102**, 100501(R) (2020).
- ⁸⁶ Also during the finalization of our paper, Z. Wang, G.-M. Zhang, Y.-F. Yang, and F.C.Zhang, Distinct pairing symmetries of superconductivity in infinite-layer nickelates, arXiv: 2006.15928 reported a theoretical study which adopts a different pairing mechanism, but attributes the difference in the pairing symmetry to the difference in the hole concentration.

Supplemental material: Designing nickelate superconductors with d^8 configuration exploiting mixed-anion strategy

Naoya Kitamine,¹ Masayuki Ochi,¹ and Kazuhiko Kuroki¹

¹*Department of Physics, Osaka University, 1-1 Machikaneyama-cho, Toyonaka, Osaka, 560-0043, Japan*
(Dated: December 2, 2020)

THE EQUIVALENCE BETWEEN THE TWO-ORBITAL MODEL AND THE BILAYER MODEL

As explained in the main text, our idea was inspired by a study on a superconducting mechanism of $\text{Ba}_2\text{CuO}_{3+\delta}$ [S1], where the near equivalence between the two-orbital model and the bilayer model[S2] plays a key role. Here, we briefly review this equivalence between the two models.

We start with a bilayer Hubbard model, where the two-layers are connected by interlayer hoppings, including the vertical hoppings t_\perp within unit cells. We label the two layers by $i = 1, 2$, and the unit cells are labeled by m . The electron-electron interaction part of the Hamiltonian of the bilayer Hubbard model, in standard notations, is given as,

$$H_{\text{int}}^{\text{bilayer}} = U \sum_m \sum_{i=1,2} n_{mi\uparrow} n_{mi\downarrow}. \quad (\text{S1})$$

Let us consider the following transformation R , which transforms the above layer representation (c) to the orbital representation (d) consisting of bonding (denoted as b) and antibonding (a) orbitals,

$$\begin{pmatrix} d_{ma\sigma} \\ d_{mb\sigma} \end{pmatrix} = R \begin{pmatrix} c_{m1\sigma} \\ c_{m2\sigma} \end{pmatrix} = \frac{1}{\sqrt{2}} \begin{pmatrix} 1 & 1 \\ -1 & 1 \end{pmatrix} \begin{pmatrix} c_{m1\sigma} \\ c_{m2\sigma} \end{pmatrix}. \quad (\text{S2})$$

Applying this transformation, (S1) becomes

$$\begin{aligned} & \frac{U}{2} \sum_{m,a} n_{ma\uparrow} n_{ma\downarrow} + \frac{U}{2} \sum_{m,a \neq b} n_{ma\uparrow} n_{mb\downarrow} \\ & - \frac{U}{2} \sum_{m,a \neq b} d_{ma\uparrow}^\dagger d_{ma\downarrow} d_{mb\downarrow}^\dagger d_{mb\uparrow} \\ & + \frac{U}{2} \sum_{m,a \neq b} d_{ma\uparrow}^\dagger d_{ma\downarrow}^\dagger d_{mb\downarrow} d_{mb\uparrow}. \end{aligned} \quad (\text{S3})$$

This is exactly the same as the on-site electron-electron interaction Hamiltonian of a two-orbital model, where the intra-orbital, inter-orbital, Hund's coupling and pair-hopping interactions are all equal to $U/2$.

As for the kinetic energy part of the bilayer model, by Fourier transforming $c_{mi\sigma}^\dagger, c_{mi\sigma}$ to $c_{\mathbf{k}i\sigma}^\dagger, c_{\mathbf{k}i\sigma}$, respectively, it can be expressed as,

$$\begin{aligned} H_{\text{kin}}^{\text{bilayer}} &= \begin{pmatrix} c_{\mathbf{k}1\sigma}^\dagger & c_{\mathbf{k}2\sigma}^\dagger \end{pmatrix} \hat{H}(\mathbf{k}) \begin{pmatrix} c_{\mathbf{k}1\sigma} \\ c_{\mathbf{k}2\sigma} \end{pmatrix} \\ &= \begin{pmatrix} c_{\mathbf{k}1\sigma}^\dagger & c_{\mathbf{k}2\sigma}^\dagger \end{pmatrix} \begin{pmatrix} \varepsilon_1(\mathbf{k}) & t_\perp + \varepsilon'(\mathbf{k}) \\ t_\perp + \varepsilon'(\mathbf{k}) & \varepsilon_2(\mathbf{k}) \end{pmatrix} \begin{pmatrix} c_{\mathbf{k}1\sigma} \\ c_{\mathbf{k}2\sigma} \end{pmatrix}. \end{aligned} \quad (\text{S4})$$

Here, the diagonal terms correspond to the kinetic energy originating from the intralayer electron hoppings, and the off-diagonal terms come from the interlayer hoppings, where we have separated the vertical hopping t_\perp , a constant, and $\varepsilon'(\mathbf{k})$, i.e., the contribution coming from other (diagonal) interlayer hoppings, which exhibits wave number dependence. Applying the transformation R , this becomes,

$$\begin{aligned} R \hat{H}(\mathbf{k}) R^\dagger &= \\ & \begin{pmatrix} \frac{1}{2}(\varepsilon_1(\mathbf{k}) + \varepsilon_2(\mathbf{k})) + \varepsilon'(\mathbf{k}) + t_\perp & \frac{1}{2}(\varepsilon_2(\mathbf{k}) - \varepsilon_1(\mathbf{k})) \\ \frac{1}{2}(\varepsilon_2(\mathbf{k}) - \varepsilon_1(\mathbf{k})) & \frac{1}{2}(\varepsilon_1(\mathbf{k}) + \varepsilon_2(\mathbf{k})) - \varepsilon'(\mathbf{k}) - t_\perp \end{pmatrix}. \end{aligned} \quad (\text{S5})$$

Now the diagonal terms are the band dispersion within each orbital, so $2t_\perp$ corresponds to the energy level off-set ΔE between the bonding and antibonding bands. The off-diagonal terms represent the hybridization between the two-orbitals; if the two layers are not equivalent, namely, $\varepsilon_2(\mathbf{k}) \neq \varepsilon_1(\mathbf{k})$, there appears hybridization between the two orbitals obtained by the transformation R , which treats the two layers equally. (Namely, R obviously does not diagonalize the kinetic energy part of the bilayer Hamiltonian.)

Conversely, viewing from the two-orbital model side, we can say from the above argument that the two-orbital model with $U = U' = J = J'$ and without hybridization between the orbitals can be transformed to a bilayer Hubbard model with appropriate intra- and interlayer hoppings, where the orbital level offset ΔE is transformed to $2t_\perp$. In actual materials, $U > U' > J \sim J'$, but the finding in Ref.[S1] and also in the present study is that the approximate equivalence between the two-orbital and bilayer models holds relatively well even for realistic values of U, U', J and J' , as far as the strong enhancement of superconductivity for large ΔE is concerned.

If orbital hybridization is present in the two-orbital model, this will give rise to an inequality of the two layers in the corresponding bilayer model, as seen from

eqn.(S5). The superconducting properties of bilayer models with inequivalent layers are not well known, to our knowledge, but we will see the effect of the orbital hybridization in the last section of this supplemental material.

LATTICE CONSTANTS AND BAND STRUCTURES

In Fig.S1 and Figs.S2-S5, we plot the lattice constants obtained by structural optimization and the band structures, respectively, for all the materials considered in the present study. The lattice constants are larger for AE and/or X with larger ionic radius, except for the case of H in the T structure. As for the band structures, the relative position between the bands reflects the tendency seen in the on-site energy of each orbital (Fig.4 of the main text).

DEPENDENCE ON THE INTERACTIONS

Here, we vary the interaction values in the five orbital model of $\text{Ca}_2\text{NiO}_2\text{Cl}_2$ in various manners and see how the eigenvalue of the Eliashberg equation is affected. In Fig.S6(a), the interactions are varied maintaining $U' = U - 2J$ so as to satisfy orbital-rotation symmetry. Within the varied parameter range, larger U results in a suppression (slight enhancement) of superconductivity for $n < 4.2$ ($n > 4.2$). From Fig.S6 (b) to (d), one of U , U' , J , J' is varied, while others are fixed. The overall tendency is that increasing U' and

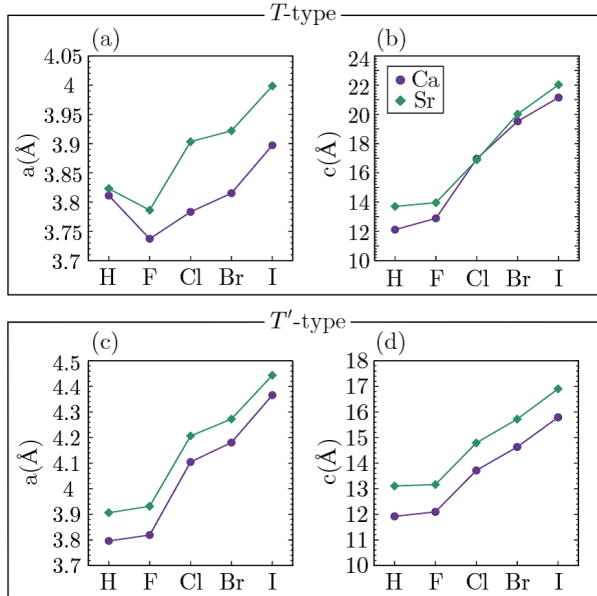


FIG. S1: Lattice constants for all the materials considered.

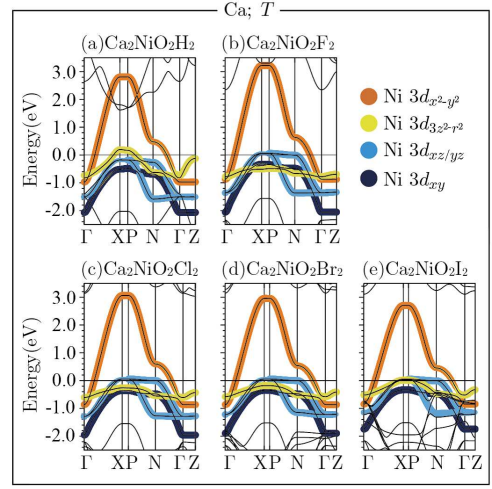


FIG. S2: Band structures of materials with $AE=\text{Ca}$ and the T structure. The band dispersion of the five orbital model is superposed to the first principles bands.

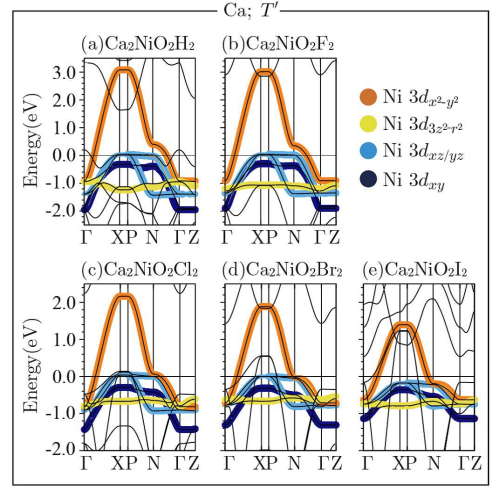


FIG. S3: Similar figure as in Fig.S2 with $AE=\text{Ca}$ and the T' structure.

J' enhances superconductivity, while increasing U and J degrades it.

STONER FACTOR FOR THE MAGNETIC ORDERING

The tendency toward magnetic ordering can be measured by calculating the Stoner factor within FLEX. In the spin-fluctuation mediated superconductivity, the Stoner factor typically becomes very close to unity (larger than 0.95, where the Stoner factor = 1 signals magnetic ordering) as the eigenvalue of the Eliashberg equation increases, which indicates that superconductivity and antiferromagnetism closely compete with each other[S3]. It is known that this is not the case for the $s\pm$ -wave super-

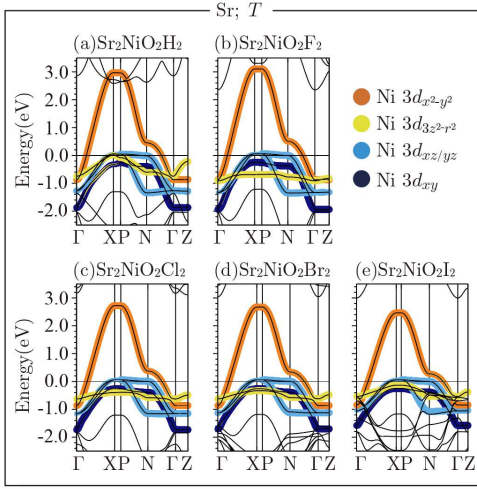


FIG. S4: Similar figure as in Fig.S2 with $AE=\text{Sr}$ and the T' structure.

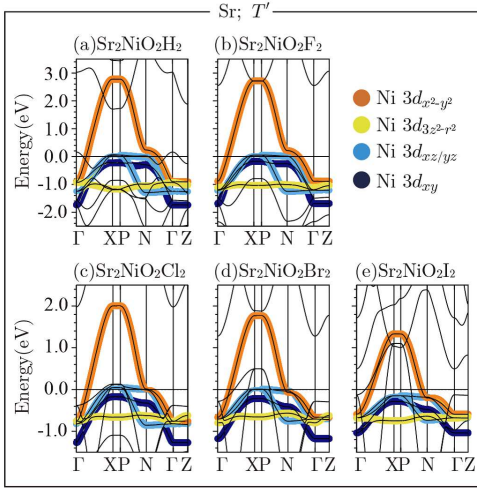


FIG. S5: Similar figure as in Fig.S2 with $AE=\text{Sr}$ and the T' structure.

conductivity enhanced by the incipient band[S4]. This is because the incipient-band mechanism exploits finite energy spin fluctuations. In fact, for the five orbital model of the proposed materials, the Stoner factor remains to stay away from unity in the parameter regime where superconductivity is optimized. As a typical example, in Fig.S7 we plot the Stoner factor calculated for the five orbital model of $\text{Ca}_2\text{NiO}_2\text{Cl}_2$ with $U = 4\text{eV}$, $J = J' = U/8$, $U' = U - 2J$, and $T = 0.01\text{eV}$.

GAP FUNCTION

In Fig.S8, we show the contour plot of the gap function for the five orbital model of $\text{Ca}_2\text{NiO}_2\text{Cl}_2$. As already seen in Fig.5(c) of the main text, this is an $s\pm$ -wave pairing with small k dependence of the gap, where

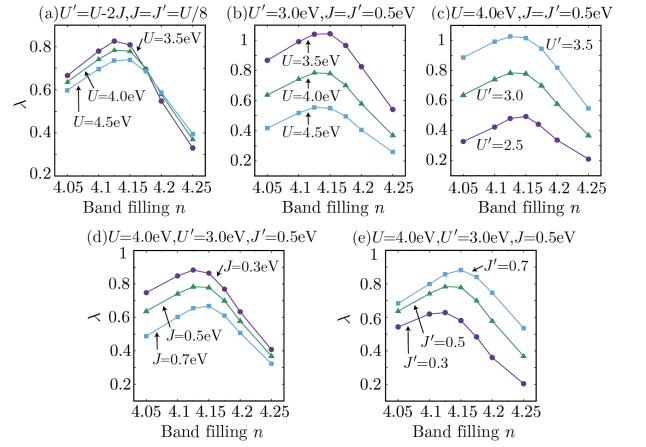


FIG. S6: Eigenvalue of the Eliashberg equation λ of the five orbital model of $\text{Ca}_2\text{NiO}_2\text{Cl}_2$ plotted against the band filling n for various sets of interaction parameters. In (a), the interactions are varied maintaining $U' = U - 2J$ so as to satisfy the orbital rotational symmetry. From (b) to (d), one of U , U' , J , J' is varied, while the others are fixed.

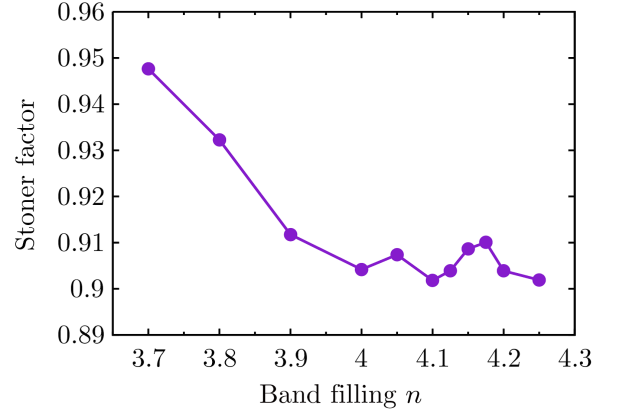


FIG. S7: The Stoner factor of the five orbital model of $\text{Ca}_2\text{NiO}_2\text{Cl}_2$ calculated at $T = 0.01\text{eV}$ within FLEX, plotted against the band filling.

the gap changes sign between the $d_{x^2-y^2}$ and incipient d orbitals. As mentioned in the main text, it is interesting to note that the $d_{3z^2-r^2}$ orbital has the largest gap function among the incipient bands despite the fact that the $d_{3z^2-r^2}$ band lies somewhat away from E_F compared to the top of the $d_{xz/yz}$ bands. This may be understood as follows. Since the gap function is barely wave-number dependent, it is likely that not just the position of the top of the band, but also the center of gravity of the incipient bands is important. Since the $d_{3z^2-r^2}$ orbital has the highest on-site energy ($|\Delta E|$ being the smallest) among the incipient orbitals in $\text{Ca}_2\text{NiO}_2\text{Cl}_2$, the $d_{3z^2-r^2}$ band can be considered as positioned closest to E_F as far as the center of gravity of the band is concerned. In fact, as shown in Fig.S9, in T' -type $\text{Ca}_2\text{NiO}_2\text{H}_2$, where the $d_{3z^2-r^2}$ orbital has the lowest on-site energy among the

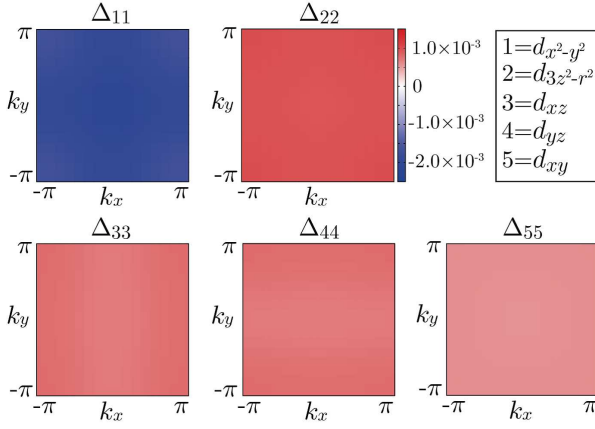


FIG. S8: Contour plot of the gap function of the five orbital model of $\text{Ca}_2\text{NiO}_2\text{Cl}_2$ for $n = 4.125$. Only the orbital diagonal components are shown.

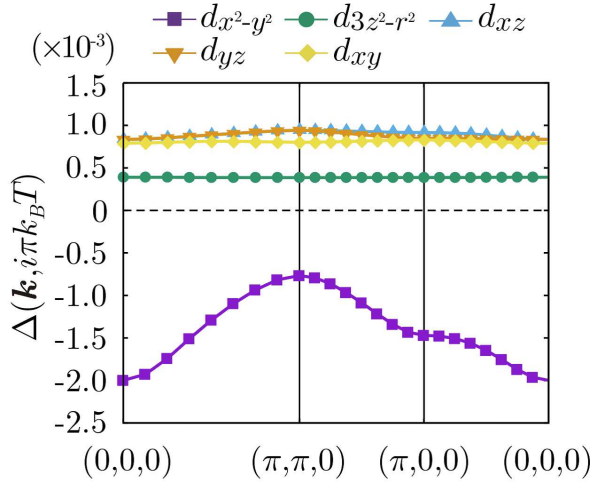


FIG. S9: The gap function of the five orbital model of $\text{Ca}_2\text{NiO}_2\text{H}_2$ for $n = 4.15$ in the orbital representation.

five orbitals, the $d_{3z^2-r^2}$ gap is found to be the smallest.

For La_2NiO_4 , there is no chance for superconductivity since λ is small, and, in the first place, we assume an unrealistic low-spin state. Nonetheless, we plot the inter-orbital and intra-orbital components of the gap func-

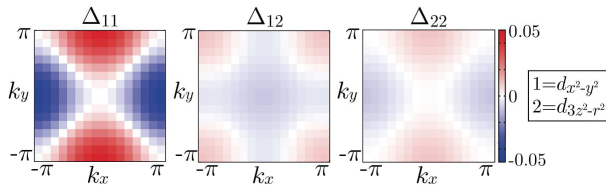


FIG. S10: Contour plot of the gap function of the five orbital model of La_2NiO_4 for $n = 4.125$. Here, we plot the off-diagonal component since it has appreciable amplitude.

tion in Fig.S10. It is mainly intra-orbital $d_{x^2-y^2}$ -wave within the $d_{x^2-y^2}$ orbital, but there is also appreciable inter-orbital component between $d_{x^2-y^2}$ and $d_{3z^2-r^2}$ orbitals. This is similar to the case of $\text{Ba}_2\text{CuO}_{3+\delta}$ studied in Ref.[S1] with small level offset between $d_{x^2-y^2}$ and $d_{3z^2-r^2}$ orbitals.

ORBITAL DECOMPOSITION

In Fig.5(d) of the main text, we compared λ of the five, four, three, and single orbital models of $\text{Ca}_2\text{NiO}_2\text{Cl}_2$ at the same electron doping rates, between 5 to 25 %. Here we explain how this is justified. In Fig.S11, we show the contour plots of $|G_{ii}(\mathbf{k}, i\pi k_B T)|^2$, where $G_{ii}(\mathbf{k}, i\pi k_B T)$ is the orbital diagonal component of the FLEX Green's function at the lowest Matsubara frequency, for the band fillings $n = 4.05, 4.1, 4.125, 4.15$, and 4.2 . The ridges of these plots represent the Fermi surfaces. We also show in Fig.S12 the position of E_F in the band structure. From this, it can be seen that beyond the band filling of $n = 4.125$ (12.5% doping), where λ is maximized, the bands other than $d_{x^2-y^2}$ sink below E_F . In Fig.S13, we show the contour plot of the squared Green's function of the $d_{x^2-y^2}$ orbital for five, four, three and single orbital models, for electron doping rates between 5 and 20 %. For 15% doping or more, where the bands other than $d_{x^2-y^2}$ sink below E_F , the $d_{x^2-y^2}$ Fermi surface is the same for all the models as expected. Even for smaller band fillings, the $d_{x^2-y^2}$ Fermi surfaces of the multiorbital models are the same because all of these models contain the $d_{xz/yz}$ orbital, which are the only orbitals other than $d_{x^2-y^2}$ that form the Fermi surfaces. Moreover, the $d_{x^2-y^2}$ Fermi surface of the multiorbital model is also similar to that of the single orbital model because the $d_{xz/yz}$ Fermi surface is very small within this electron doping range. In a nutshell, the comparison of the multiorbital and single orbital models at the same electron doping rates is justified because the $d_{x^2-y^2}$ Fermi surfaces of these models are (nearly) the same.

From the above analysis, it can also be understood why we have considered, in Fig.5(d) of the main text, only models that contain the $d_{xz/yz}$ orbitals (except for the single orbital model). Since the top of the $d_{xz/yz}$ bands has the highest energy among the bands other than $d_{x^2-y^2}$ and the Fermi level for the stoichiometric band filling of $n = 4$ intersects only the $d_{x^2-y^2}$ and $d_{xz/yz}$ bands, the Fermi level of the full five orbital model with the band filling of $n(\geq 4)$ is the same as that of an n_{orb} orbital model with the band filling of $n - (5 - n_{\text{orb}})$, as far as the models that contain the $d_{xz/yz}$ orbitals are concerned. Conversely, the Fermi level of, say, a two-orbital $d_{x^2-y^2} + d_{xy}$ model with the band filling of $n - 3$ is not the same as that of the full five orbital model with the band filling of n . Hence, such models were not considered in the main text. Nonetheless, it is interesting to

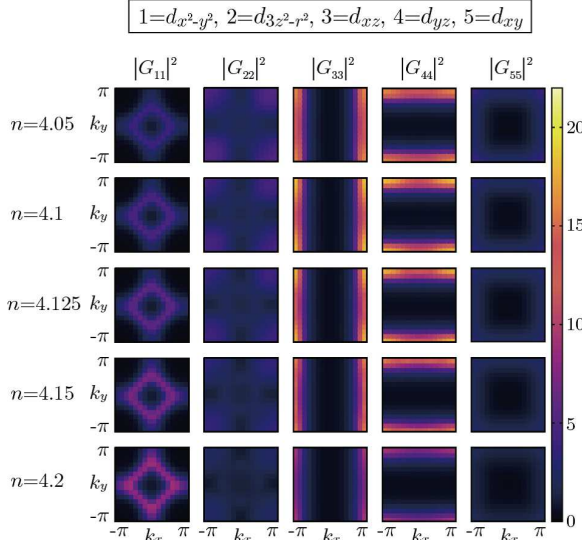


FIG. S11: Contour plots of $|G_{ii}(\mathbf{k}, i\pi k_B T)|^2$ for the five orbital model of $\text{Ca}_2\text{NiO}_2\text{Cl}_2$ for $n = 4.05, 4.1, 4.125, 4.15$, and 4.2 .

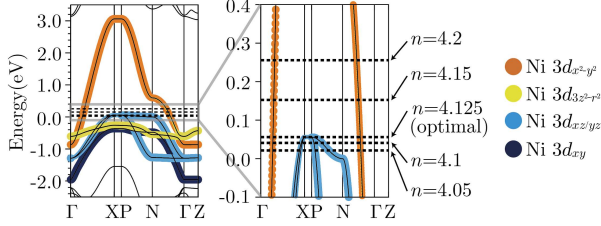


FIG. S12: The band structure of the five orbital model of $\text{Ca}_2\text{NiO}_2\text{Cl}_2$, together with the position of E_F for $n = 4.05, 4.1, 4.125, 4.15$, and 4.2 . Note that this is the bare band structure, but the Fermi surfaces themselves are not affected by the interaction since the real part of the self-energy at $\omega = 0$ is subtracted in the FLEX calculation.

study how each band would affect superconductivity if other bands were absent. In Fig.S14, we plot the eigenvalue of the Eliashberg equation against the band filling for two-orbital $d_{x^2-y^2} + d_{xy}$ and $d_{x^2-y^2} + d_{3z^2-r^2}$ models, in addition to the $d_{x^2-y^2} + d_{xz/yz}$ model, the single orbital $d_{x^2-y^2}$ model, and the full five orbital model. It can be seen that all of the bands can act as an incipient band that enhances $s\pm$ superconductivity compared to the single orbital case. A tendency here is that the orbitals having larger $|\Delta E|$ (level offset with respect to the $d_{x^2-y^2}$ orbital, corresponding to $2t_\perp$ in the bilayer Hubbard model) give stronger enhancement of superconductivity, and superconductivity is optimized at lower band fillings. This tendency is indeed the same as that seen in the bilayer Hubbard model[S5–S7].

Here we also comment on the comparison of the gap function among the multiorbital models. In Fig.S15(a),

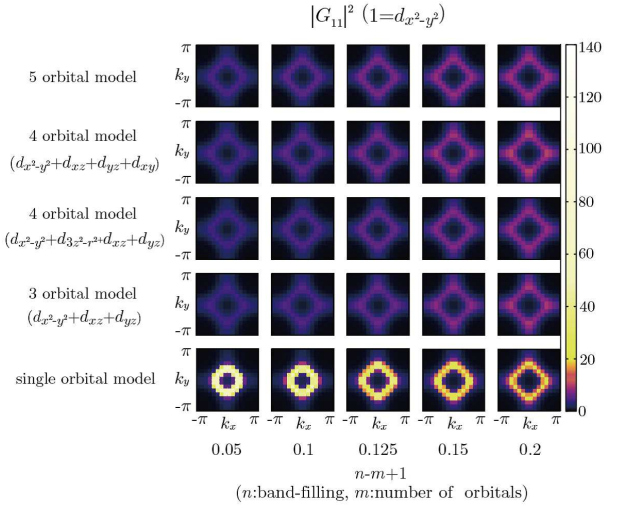


FIG. S13: Contour plots of $|G_{ii}(\mathbf{k}, i\pi k_B T)|^2$ with $i = d_{x^2-y^2}$ orbital for five, four (two-types), three, and single orbital models of $\text{Ca}_2\text{NiO}_2\text{Cl}_2$ for various electron doping rates.

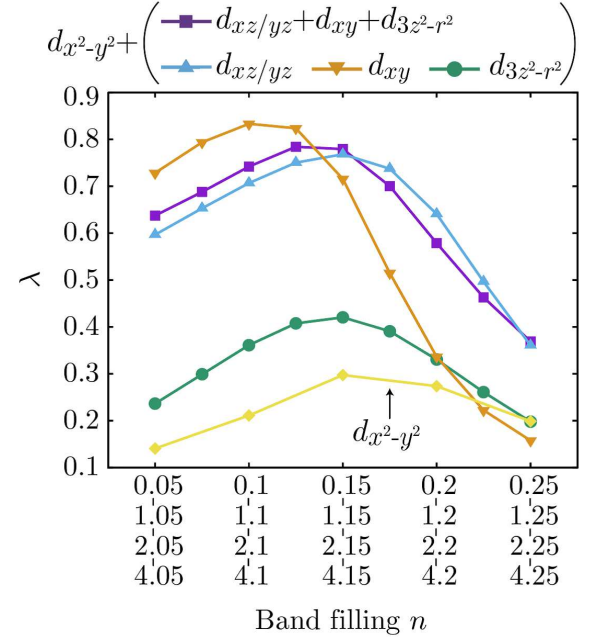


FIG. S14: λ against the band filling for various models of $\text{Ca}_2\text{NiO}_2\text{Cl}_2$.

we show the gap function of the $d_{x^2-y^2} + d_{xz/yz}$ model for $n = 2.15$. This gap function exhibits wave number dependence for the $d_{x^2-y^2}$ orbital, which differs from the case of the bilayer Hubbard model, where the gap function barely varies against the wave number. Similar difference between the two-orbital model and the bilayer model was pointed out in Ref.[S1], and was attributed to the inequality among the interactions, i.e., $U \neq U' \neq J$. Interestingly, as shown in Fig.S15(b), in the five orbital model, this wave number dependence is suppressed, and

the gap function looks closer to that of the bilayer Hubbard model. The reason for this is not clear at present, and remains as an interesting future problem.

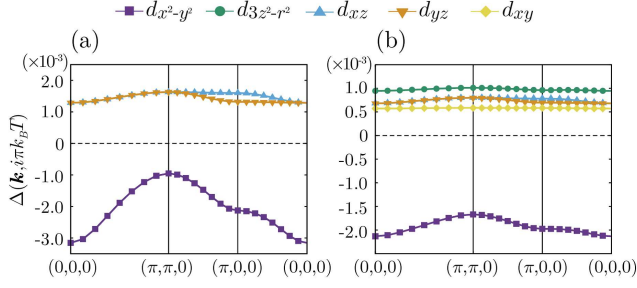


FIG. S15: The gap function of (a) the $d_{x^2-y^2} + d_{xz/yz}$ model ($n = 2.15$) and (b) the five orbital model ($n = 4.125$) of $\text{Ca}_2\text{NiO}_2\text{Cl}_2$.

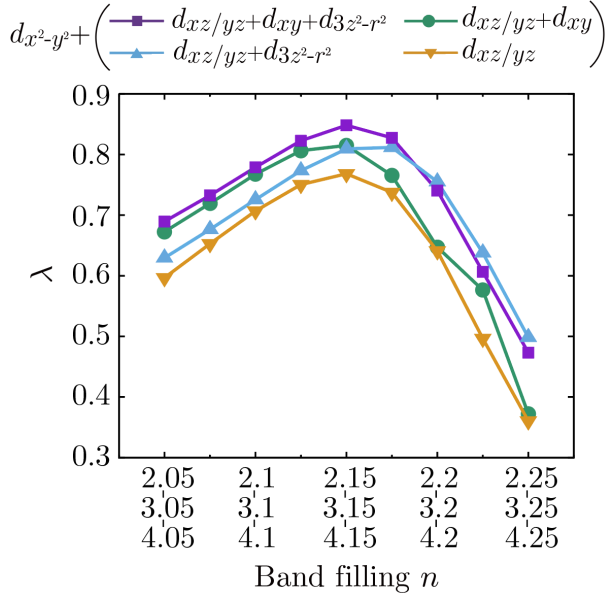


FIG. S16: λ against the band filling for various models of $\text{Ca}_2\text{NiO}_2\text{Cl}_2$. Here, the hybridization between the $d_{3z^2-r^2}$ and $d_{x^2-y^2}$ orbitals is turned off.

THE EFFECT OF THE ORBITAL HYBRIDIZATION

In Fig.S14, the enhancement of superconductivity in the $d_{x^2-y^2} + d_{3z^2-r^2}$ model appears to be rather small

even considering the small $|\Delta E|$ of the $d_{3z^2-r^2}$ orbital. Moreover, as seen in Fig.5(d) of the main text, adding $d_{3z^2-r^2}$ to $d_{x^2-y^2} + d_{xz/yz}$ suppresses λ , while adding the d_{xy} orbital to the $d_{x^2-y^2} + d_{xz/yz}$ model enhances it. The difference between $d_{3z^2-r^2}$ and d_{xy} lies in that the former orbital hybridizes with $d_{x^2-y^2}$. In fact, as shown in Fig.S16, if we hypothetically turn off the hybridization, we find that adding $d_{3z^2-r^2}$ to $d_{x^2-y^2} + d_{xz/yz}$ or to $d_{x^2-y^2} + d_{xz/yz} + d_{xy}$ actually enhances λ . Similarly, it was also found in the two-orbital model in Ref.[S1] that turning off the hybridization enhances superconductivity when one of the bands is incipient. As described in the first section of this supplemental material, the presence of the orbital hybridization in the two-orbital model results in an inequivalence of the two layers when transformed into the bilayer model. We believe that this should be related to the suppression of superconductivity in the presence of the hybridization, although more study on this issue is necessary for further clarification.

-
- [S1] K. Yamazaki, M. Ochi, D. Ogura, K. Kuroki, H. Eisaki, S. Uchida, and H. Aoki, Superconducting mechanism for the cuprate $\text{Ba}_2\text{CuO}_{3+\delta}$ based on a multiorbital Lieb lattice model, *Phys. Rev. Research* **2**, 033356 (2020).
 - [S2] H. Shinaoka, Y. Nomura, S. Biermann, M. Troyer, and P. Werner, Negative sign problem in continuous-time quantum Monte Carlo: Optimal choice of single-particle basis for impurity problems, *Phys. Rev. B* **92**, 195126 (2015).
 - [S3] See, e.g., R. Arita, K. Kuroki, and H. Aoki, *d*- and *p*-wave superconductivity mediated by spin fluctuations in two- and three-dimensional single-band repulsive Hubbard model, *J. Phys. Soc. Jpn.* **69**, 1181 (2000).
 - [S4] D. Ogura, Springer Theses, "Theoretical study of electron correlation driven superconductivity in systems with coexisting wide and narrow bands", Springer (2019).
 - [S5] T. Maier and D.J. Scalapino, Pair structure and the pairing interaction in a bilayer Hubbard model for unconventional superconductivity, *Phys. Rev. B* **84**, 180513(R) (2011).
 - [S6] K. Matsumoto, D. Ogura and K. Kuroki, Strongly enhanced superconductivity due to finite energy spin fluctuations induced by an incipient band: A FLEX study on the bilayer Hubbard model with vertical and diagonal interlayer hoppings, *J. Phys. Soc. Jpn.* **89**, 044709 (2020).
 - [S7] D. Kato and K. Kuroki, Many-variable variational Monte Carlo study of superconductivity in two-band Hubbard models with an incipient band, *Phys. Rev. Research* **2**, 023156 (2020).